Polymer Bulletin (2023) 80:9853–9880
https://doi.org/10.1007/s00289-022-04536-0

ORIGINAL PAPER

Synthesis, characterization and affinity detection of sulfonated polyimides: confirmation of proton transfer in quantum theory simulations

Aslihan Aycan Tanriverdi[1] · Umit Yildiko[2] · Ahmet Turan Tekes[1] · İsmail Cakmak[1] · Ahmet Cagri Ata[1]

Received: 17 January 2022 / Revised: 21 September 2022 / Accepted: 15 October 2022 /
Published online: 29 October 2022

Abstract

Here, two different novel sulfonated polyimides were produced using different monomer ratios. With 2 different molecules of diamine, 3,3′,4,4′-biphenyl tetracarboxylic dianhydride and perylene-3, 4, 9, 10-tetracarboxylic dianhydride in an inert atmosphere at two-stage high temperature and the presence of sulfonic acid, sulfonated polyimides were obtained by imidization. For sulfonated polyimides, proton nuclear magnetic resonance, Fourier transform infrared, solubility tests, the affinity of polymers to solvents, ultraviolet–visible spectroscopy and thermogravimetric analysis/differential thermal analysis characterization were performed. Quantum chemical calculations of synthesized sulfonated polyimides, density functional theory and analysis of atoms in molecules theoretical calculations are presented to learn about various energy properties and to see proton transfer scripts. The thermogravimetric analysis/differential thermal analysis curve showed a second degradation stage at a temperature higher than 400 °C.

✉ Umit Yildiko
yildiko1@gmail.com

[1] Faculty of Arts and Sciences. Department of Chemistry, Kafkas University, 36100 Kars, Turkey

[2] Engineering and Architecture Faculty. Department of Bioengineering, Kafkas University, 36100 Kars, Turkey

Graphical abstract

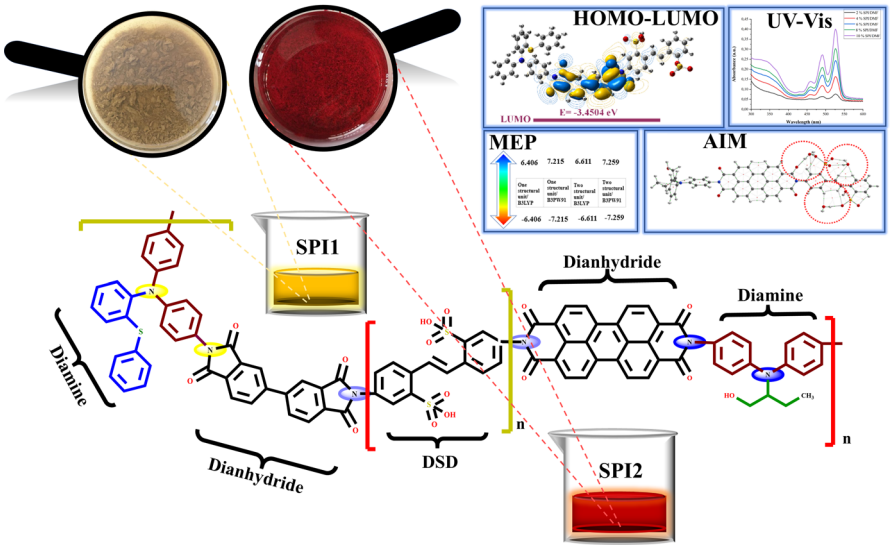

Keywords Diamine · Sulfonated polyimide · Solubility · Affinity · Dipole moment · DFT · AIM

Introduction

Polyimides (PIs), which are polymers with good potential, are used in making materials in many areas [1]. PIs represent the most studied class of high-performance polymers [2]. They are more commonly known as membrane polymers because of their superior properties and because they can be packaged in modules with high surface area, they are thin and flawless, and they are also low cost [3]. PIs are synthesized as a result of the condensation of poly(amic acid) [4] which consists of the reaction of a dianhydride and a diamine or its derivatives in a solvent environment [5]. In addition, when more than two monomers are used, copolyimides are formed. PIs can be classified according to processability or polymer chain [6]. PIs can be classified as thermoplastic and thermoset PIs according to their machinability. Thermoplastic PIs can be processed by standard methods. Thermoset PIs are polymers that are generally obtained as a result of addition or condensation polymerization and decompose before reaching the melting point during processing and are resistant to high temperatures [7]. PIs synthesized from aromatic monomers are generally insoluble and difficult to process. Aromatic PIs provide their high thermal and mechanical strength and high dielectric constants with the charge transfer complex [8]. Today, it has been desired to produce new variations of the high-temperature, low-cost and stable membrane [9]. Most of the alternative membranes were selected from polymers with aromatic structures [10]. The doped or functional state of

aromatic polymers is suitable to make them proton conductors [11]. The generally preferred method is functionalization by grafting sulfonic acid. As an alternative, it became necessary to search for high-performing polymers [12]. Many sulfonated hydrocarbon polymers have been investigated. It has been determined that SPI [13, 14] were favorable materials for proton exchange application [15–17]. On the other hand, SPIs have high chemical, thermal and mechanical resistance due to their similarity with PI (although filled with electrolyte during the hydration condition, it is inert, does not swell, is widely used in electronic devices, is not permeable to methanol and is heat resistant (− 269 to + 400 °C)) [18].

The behavior of a polymer toward solvent and polymers is significant. Polymer–solvent affinity is driven by both the strength of the interaction between them and the entropy change that takes place during mixing [19, 20]. The most common way to estimate polymer–solvent affinity is with Hildebrand solubility parameters (δ), introduced in 1950 [21, 22]. The solubility parameters (δ) of polymers or solvents describe the attractive force between molecules of a similar kind. It is defined as the square root of the cohesion energy density. It is also related to the evaporation energy per unit volume in solvents [21].

In this study, two new sulfonated polyimides (SPI1 and SPI2) were synthesized. 3,3′,4,4′-Biphenyl tetracarboxylic dianhydride (BPDA) and perylene-3,4,9,10-tetracarboxylic dianhydride (PTCDA) were used as sources of aromatic groups in the synthesis. In line with the popularity of SPIs in recent years and the need for new polyimides, it has been deemed necessary to gain new scientific data with both experimental and theoretical studies. The results obtained supported the formation of SPI. In addition, affinity calculations were carried out to support the experimental solubility tests to determine the solubility parameters. Quantum chemical calculations of some of the units of the polymers at the oligomer level have been studied. The energy calculations of the obtained polymers were investigated using the density functional theory (DFT) method. In addition, analysis of atoms in molecules (AIM) was carried out in a structural unit of SPIs.

Experimental

Materials

2-(Phenylthio)aniline (≥ 98.0%, Sigma-Aldrich), 2-amino-1-butanol (98% Sigma-Aldrich), 4-fluoronitrobenzene (99%, Sigma-Aldrich), cesiumfluoride (99%, Sigma- Aldrich), dimethyl sulfoxide (DMSO) (Merck), ethanol (EtOH) (99.8%, Sigma-Aldrich), acetic acid (100%, Merck), Pd/C (10%) (Sigma-Aldrich), hydrazine monohydrate (Sigma-Aldrich), diethyl ether/petroleum ether (1:1) (Sigma-Aldrich), 4,4′-diamino-2,2′-stilbenedisulfonic acid (DSD) (Sigma-Aldrich), *m*-Cresol (99%,Sigma-Aldrich), triethylamine (99.5%, Sigma-Aldrich), perylene-3,4,9,10-tetracarboxylic dianhydride (PTCDA) (97%, Sigma-Aldrich), 3,3′,4,4′- biphenyltetracarboxylic dianhydride (BPDA) (97%, Sigma-Aldrich), benzoic acid (Merck), ethyl acetate (Sigma-Aldrich), acetone (Sigma-Aldrich), *N*-methyl-2-pyrrolidone (NMP) (Sigma-Aldrich), dimethylacetamide (Dmac) (≥ 99.0%, Sigma-Aldrich),

N,*N*-dimethylformamide (DMF) (Sigma-Aldrich), chloroform ($CHCl_3$) (Sigma-Aldrich), dichloromethane (CH_2Cl_2) (Sigma-Aldrich), toluene (99.8%, Sigma-Aldrich) and tetrahydrofuran (THF) (Sigma-Aldrich) were purchased and used in experimental processes.

Characterization and simulations of the analysis

The density of PIs was determined by the pycnometer method in the presence of acetone. ^{1}H-NMR Bruker Avance III HD 600 MHz model device (Germany) was used for the structural illumination of the compounds. NMR spectroscopic required data were recorded in DMSO following deuterium-free signal internal standards for proton nuclear magnetic resonance (^{1}H-NMR). The IR spectrum was acquired on a PerkinElmer spectrum on a Fourier transform infrared (FT-IR) spectrophotometer to express shifts. Ultraviolet–visible spectroscopy (UV–Vis) analysis was performed directly with skanlt software and Multiskan Sky microplate spectrophotometer with the cuvette reader model. For thermogravimetric analysis (TGA)/differential thermal analysis (DTA), thermal analysis measurements of the polymers were made using a TGA/DTA 1600 to determine thermal degradation. All structural units were drawn in ChemDraw. The drawn molecules were converted to 3D MOL2 file type in Chem3D [23]. In DFT studies on one structural unit and two structural units of SPI1 and SPI2, MOL2 files were transferred to Gaussian 09 W software, revision B.01. One and two structural units of SPI1 and SPI2 were optimized in the singlet state. Then, quantum chemical calculations of the optimized structures were performed using the valence polarized basis set 6-311G together with the hybrid density functional B3LYP. Likewise, the B3PW91 functional with the 6-311G(d, p) basis set was used to compare with this anecdote. In addition, the values of HOMO and LUMO energies and the values of HOMO/LUMO spaces were used to calculate the values of global reactivity parameters (GRP). In addition, β, electric dipole moment (μ) and polarizability ($\Delta\alpha$) were determined to examine the NLO behavior. GaussView 5.0 program was used to visualize all studies and MEPs of DFT calculations [24]. One structural unit of SPI1 and SPI2 were added separately to the structure with 0, 1, 2 and 3 water molecules in Gaussian 09 W software. Then, checkpoint files were prepared using the B3LYP/6-311G functional. These files were converted to formatted checkpoint file type and transferred to the AIMQB system of the AIMAII program, and the program was run. Then, the parameters (values in the tables) of the AIM analysis in the literature were calculated in the AIMStudio system connected to this program and their images were taken [25].

Synthesis of N^1-(4-aminophenyl)-N^1-(2-(phenylthio)phenyl)benzene-1,4-diamine (Diamine 1) and 2-(bis(4-aminophenyl)amino)butan-1-ol (Diamine 2)

2-(Phenylthio) aniline 12 g (30 mmol) and 2-amino-1-butanol 2.67 g (30 mmol) were put into two three-necked 250-mL glass flasks. 4-Fluoro nitrobenzene 16.92 g (60 mmol) and cesium fluoride 17.4 g (60 mmol) were dissolved in 50 mL DMSO and stirred at 115 °C for 14 h in a nitrogen atmosphere in separate balloons.

The flask with the mixture was precipitated in 400 mL of ethanol after cooling to 24 °C. The yellow precipitate was filtered using a gouch funnel, dried under vacuum and finally crystallized with acetic acid. As a result of these two reactions, 10 mmol (4.1 g) 2-phenylthio aniline and 10 mmol (4.1 g) 2-(bis(4-nitrophenyl)amino) butan-1-ol are formed. These two monomers were then added again to two identical three-necked 250 mL glass balloons. Then, 0.10 g of Pd/C (10%) was added to each flask separately, followed by 85 mL of EtOH. Balloons and mixtures were heated to boiling temperature. Immediately afterward, a solution of 30 mmol (1.16 g) hydrazine monohydrate in 20 mL of ethanol was added dropwise and stirred under reflux for 20 h. The reaction mixture was cooled to 25 °C. Pd/C (10%) was filtered using filter paper and removed. The solvent in the mixture was evaporated under a vacuum on the evaporator. It was precipitated in diethyl ether/petroleum ether (1:1) and the mixture was filtered in a crucible. Finally, it was dried in a vacuum oven at 50 °C [26] (Fig. 1). Yield 3.52 g (67%) for diamine 1. Yield 3.47 g (66%) for diamine 2 [27]. Diamine 1 was newly synthesized. For *N*,*N*-bis(4-nitrophenyl)-2-(phenylthio) aniline, ^{1}H-NMR (400 MHz, Chloroform-*d*) δ 8.23–8.11 (m, 3H), 7.41–7.21 (m, 6H), 7.21–7.08 (m, 4H), 7.04 (s, 1H) (Fig. S1). ^{13}C-NMR (101 MHz, Chloroform-*d*) δ 150.86, 142.67, 141.62, 138.15, 133.56, 131.87, 131.62, 130.38, 129.62, 129.13, 128.72, 128.30, 125.46, 121.18 (Fig. S2). For diamine 1, ^{1}H-NMR (400 MHz, Chloroform-*d*) δ 8.22–8.11 (m, 1H), 8.10–7.98 (m, 1H), 7.44–7.03 (m, 8H), 6.77–6.56 (m, 2H) (Fig. S3). ^{13}C-NMR (101 MHz, Chloroform-*d*) δ 153.75, 150.86, 144.99, 142.68, 139.15, 137.75, 133.72, 133.57, 130.74, 130.37, 129.89, 129.63, 129.49, 129.13, 128.73, 128.37, 128.01, 127.89, 127.71, 125.65, 125.47, 121.18, 115.99, 115.02 (Fig. S4).

Polyimide synthesis (SPI1) with BPDA and diamine 1

To the 250-mL flask were, respectively, added 0.22 g (0.6 mmol) DSD, 0.246 g (0.6 mmol) diamine 1, 6 mL m-Cresol and 0.4 mL triethylamine under nitrogen flow. After DSD and diamine 1 were completely dissolved, 0.352 g (1.2 mmol) BPDA and 0.173 g benzoic acid were added to the mixture. It was then stirred at 24 °C for a few minutes and then heated at 80 °C for 5 h to obtain polyamic acid (PAA). The resulting PAA was then heated at 190 °C for one day. 10 mL of *m*-Cresol was added to the mixture to further dilute the viscous solution. The solution was precipitated in ethyl acetate. The precipitated PI was collected by filtration through filter paper and washed with acetone. Finally, it was vacuum-dried at 50 °C for 16 h (Fig. 2). FT-IR (υ, cm^{-1}): 1771 and 1717 (C=O), 1483 (aromatic C-H), 1355 (aromatic C=C), 1229 (pi-substituted C=C), 1152 (S-O), 1074 (C-N). ^{1}H-NMR (400 MHz, Chloroform-*d*) δ 8.25–8.10 (m, 3H), 7.41–7.21 (m, 4H), 7.21–7.08 (m, 4H), 7.04 (s, 1H).

Polyimide Synthesis (SPI2) with PTCDA and Diamine 2

To the 250-mL flask were, respectively, added 0.22 g (0.6 mmol) DSD, 0.162 g (0.6 mmol) diamine 2, 6 mL m-Cresol and 0.4 mL triethylamine under nitrogen

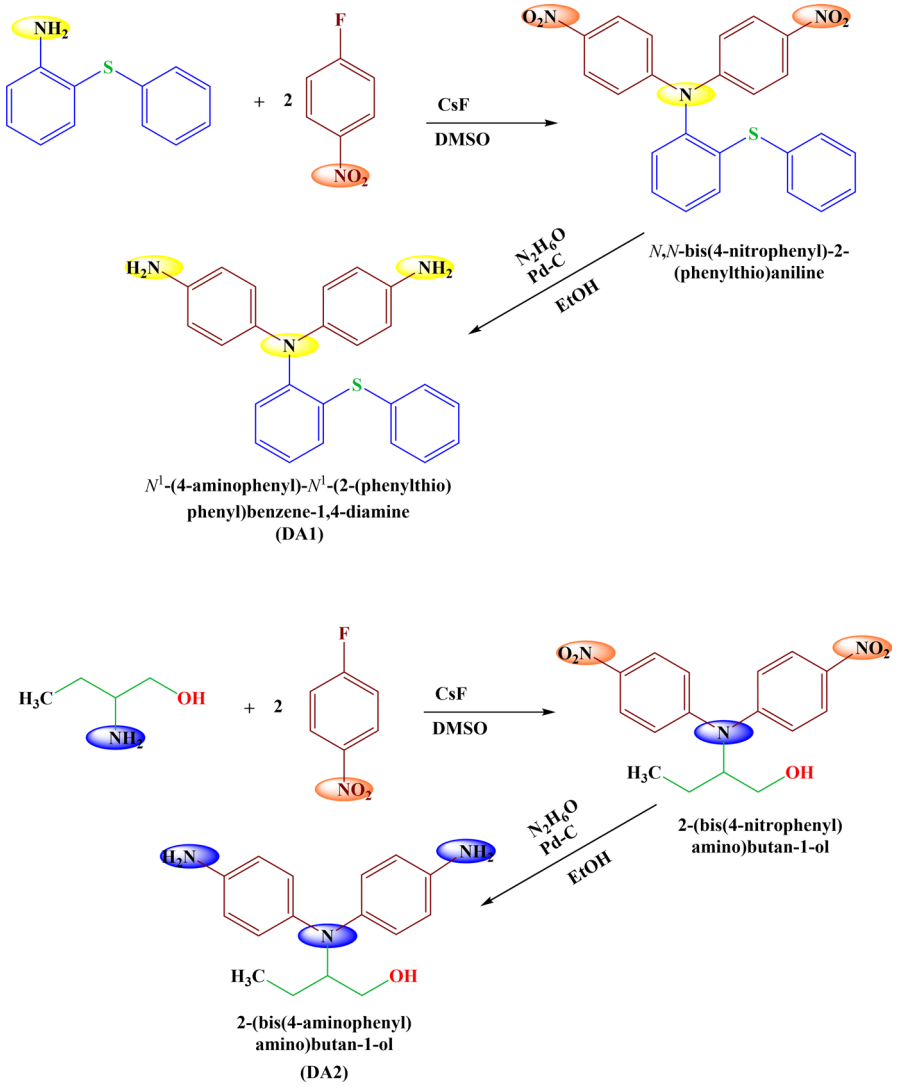

Fig. 1 Synthesis schemes of diamine 1 and diamine 2

flow. After DSD and diamine 2 were completely dissolved, 0.470 g (1.2 mmol) PTCDA and 0.173 g benzoic acid were added to the mixture. The same processes as in SPI1 were applied (Fig. 3). FT-IR (υ, cm^{-1}): 1762 and 1698 (C = O), 1537 (aromatic C-H), 1479 (C-C), 1297 (aromatic C = C), 1228 cm^{-1} (pi-substituted C = C), 1348 (C-N), 1147 (S–O). ^{1}H-NMR (400 MHz, DMSO-d_6) δ 9.43 (s, 2H), 9.18 (d, J = 11.8 Hz, 1H), 6.85 (s, 4H), 6.62–6.52 (m, 2H), 3.04 (s, 1H), 2.48 (s,

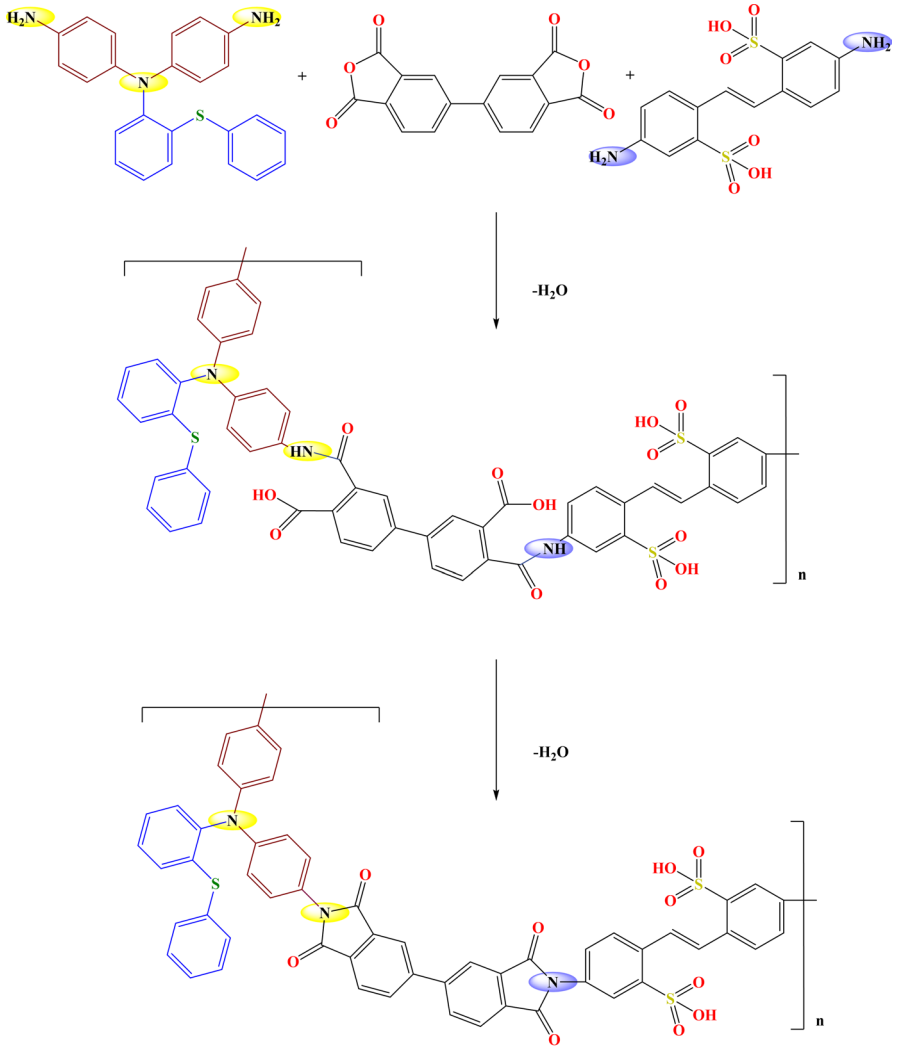

SPI1

Fig. 2 Synthesis scheme of SPI1

1H), 2.34 (s, 7H), 2.20 (d, $J = 10.2$ Hz, 2H), 1.30 (s, 10H), 1.16 (s, 3H), 1.15 (d, $J = 8.1$ Hz, 1H).

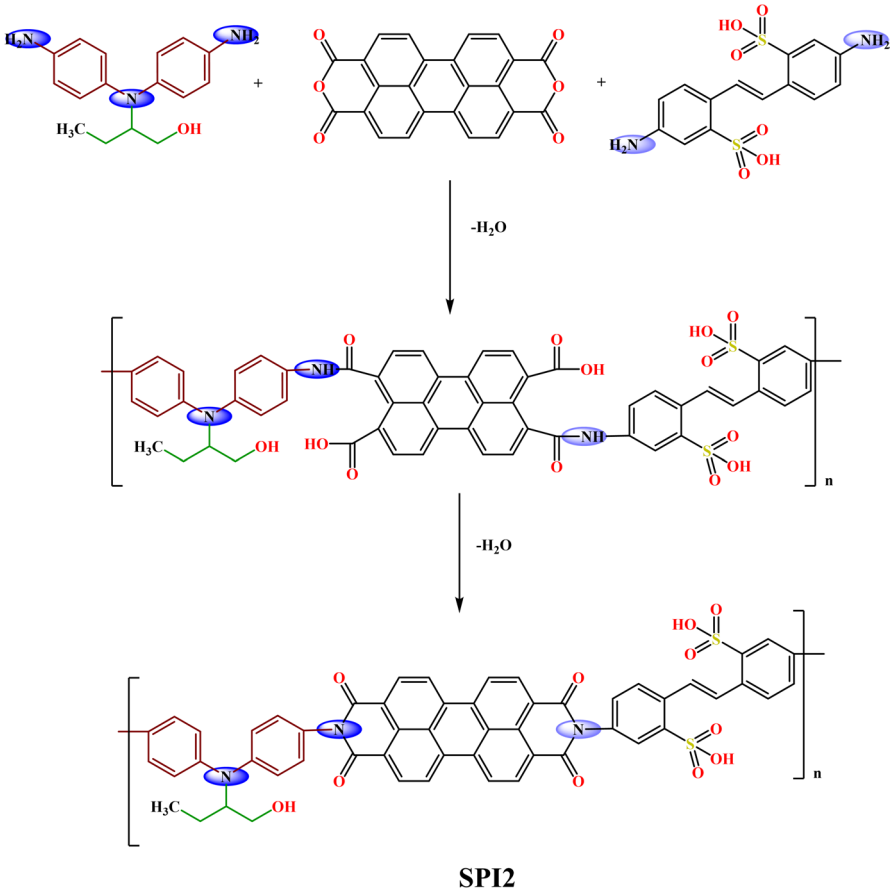

Fig. 3 Synthesis scheme of SPI1

Results and discussion

Characterization of polyimide SPI1 and SPI2

^{1}H-NMR spectrum of SPI1 and SPI2

^{1}H-NMR is very favorable for advanced methods such as spin diffusion, energy transfer, excimer fluorescence, depolarization current and neutron scattering [28–30]. ^{1}H-NMR spectra are recorded with DMSO as standard at frequencies of 400 MHz. For analysis, the compounds were converted to the presulfonated form. ^{1}H-NMR also gives knowledge about proton mobility and hydrogen bonding. The fact that the proton movement of the solid-state polyelectrolyte is linked to the chain dynamics, on the one hand, and the proton conduction determines, on the other hand, is essential to understanding the PEM transport mechanism, since

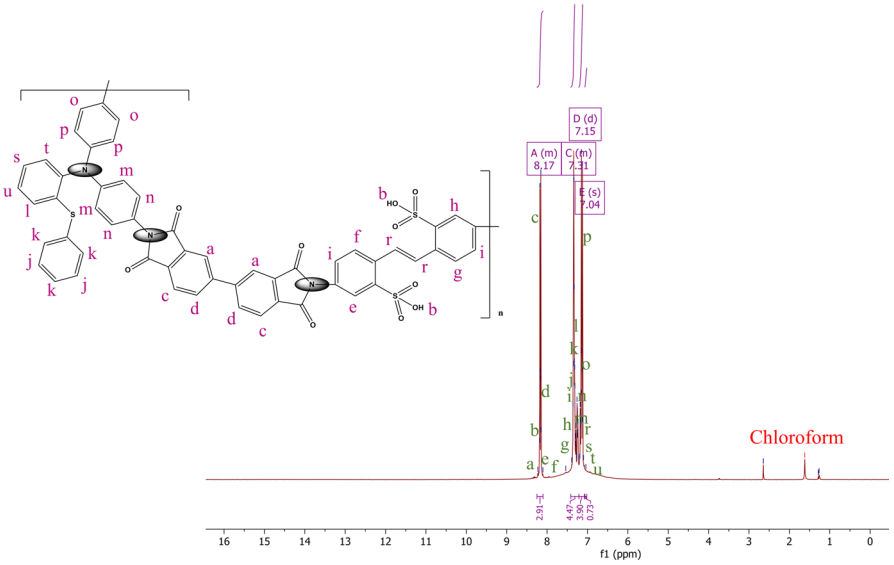

Fig. 4 [1]H-NMR spectra of SPI1

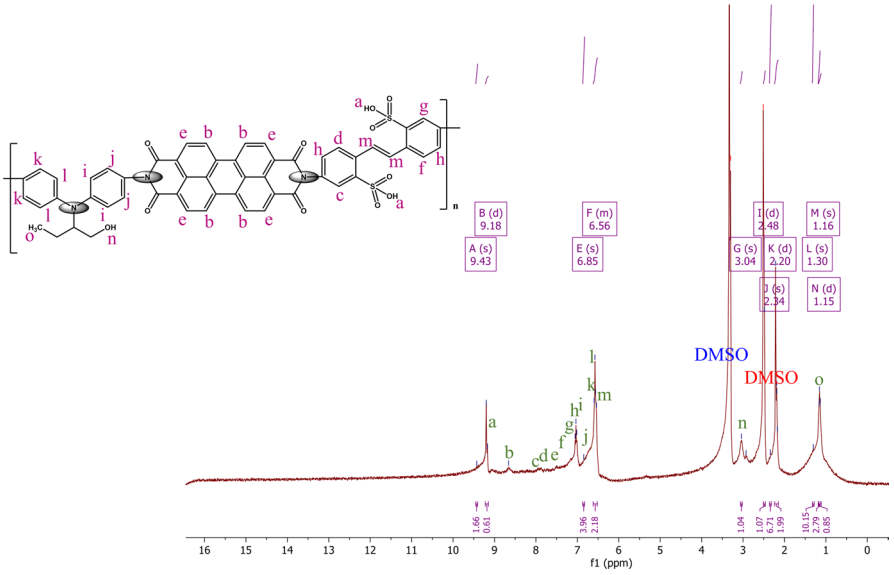

Fig. 5 [1]H-NMR spectra of SPI2

the proton movement of the solid-state polyelectrolyte is also linked to the chain dynamics [31]. Figures 4 and 5 show the [1]H-NMR spectra of the different polymers SPI1 and SPI2. In SPI1 is the peak of H-C = C aromatic of 8.33–8.28 ppm BPDA, SO_3H of 8.31 ppm DSD. On the other hand, the peaks at 8.02–8.00 ppm

and 7.96–7.94 ppm showed the H-C = C aromatic shift of DSD. At the same time, protons (H-C = C, aromatic) attributed to diamine 1 between 7.55–6.90 ppm reflect. Finally, chemical shifts of HC = CH protons at 7.25 ppm are attributed to DSD.

In SPI2, it reflected the protons of SO_3H belonging to 9.20 ppm DSD. The broad peak of 9.18 ppm and 7.03 ppm showed the H-C = C aromatic protons of PTCDA. Peaks between 7.06–7.04 ppm and 7.02–6.98 ppm indicated the H-C = C aromatic shift of DSD. In addition, peaks between 6.65–650 ppm presented protons of diamine 2 (H-C = C, aromatic). 2.51 ppm is attributed to the -OH proton of diamine 2 and 1.15 ppm to the -CH3 proton of diamine 2. Finally, the chemical shifts of HC = CH protons at 6.55 ppm belong to DSD. In conclusion, the successful preparation of SPI1 and SPI2 polymers has been demonstrated based on the above results.

FT-IR spectrum of SPI1 and SPI2

FT-IR analysis is performed to determine the hydrophilic properties of the sulfonic acid group and the stretching vibrations of the functional groups. In addition, it can be understood from the FT-IR spectrum whether the synthesis was successful or not. In FT-IR spectra, it serves to confirm the introduction of imide moieties into chain backbones in characteristic structure determination such as group absorptions (symmetric stretching, asymmetric stretching and atom–atom stretching) [32, 33]. Figures 6 and 7 show the FT-IR analysis of SPI1 and SPI2, with different peaks observed for the corresponding functional groups. In the spectrum for SPI1, the absorption peak at 3237 cm^{-1} showed HO adsorbed by SPI1 as the sulfonic acid

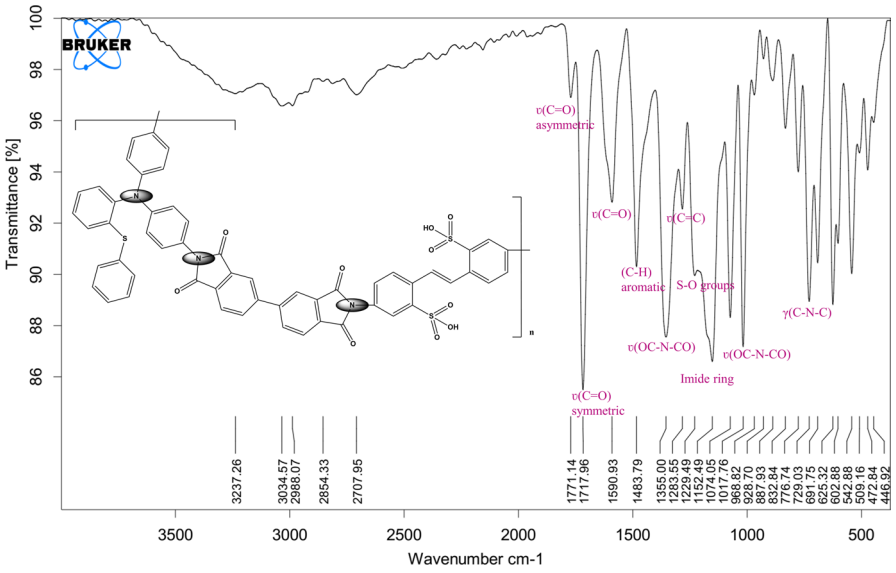

Fig. 6 FT-IR spectra of SPI1

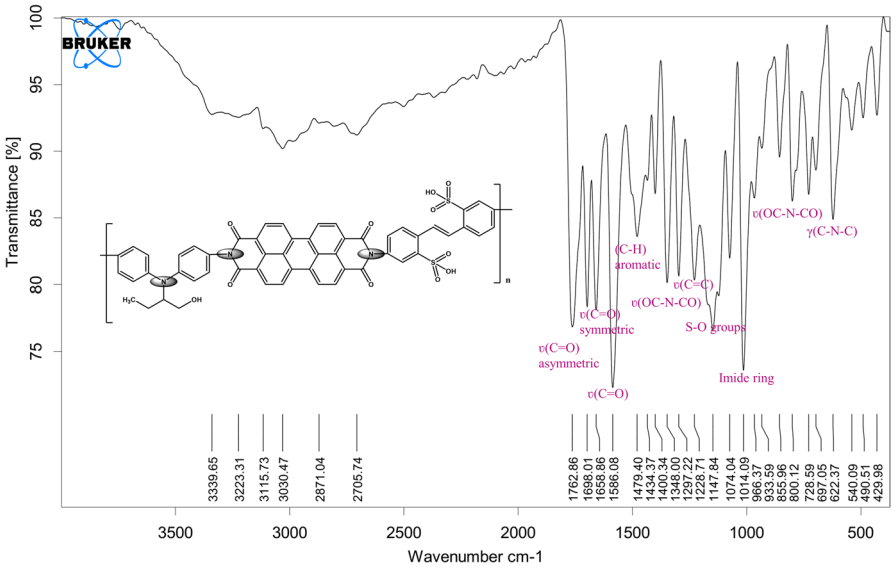

Fig. 7 FT-IR spectra of SPI2

group is hydrophilic. A small peak of 1771 cm^{-1} (C=O asymmetric stress) and a large peak of 1717 cm^{-1} (C=O symmetrical stress) appeared. In 1483 cm^{-1} (aromatic CH), 1355 cm^{-1} (C=C stretch of aromatic), 1229 cm^{-1} (C=C stretch of p-substituted benzene) and 1152 cm^{-1} (SO groups) SPI groups showed peaks.

In the spectrum for SPI2, the absorption peak at 3339 cm^{-1} indicated H_2O adsorbed by SPI2 as the sulfonic acid group is hydrophilic. A small peak of 1762 cm^{-1} (C=O asymmetric stress) and a large peak of 1698 cm^{-1} (C=O symmetrical stress) appeared. At 1479 cm^{-1} (aromatic C-H), 1297 cm^{-1} (C=C stretch of aromatic), 1228 cm^{-1} (C=C stretch of p-substituted benzene) and 1147 cm^{-1} (SO groups) showed SPI groups.

Solubility test of SPI1 and SPI2

Good solubility is one of the significant parameters for industrial applications of SPIs obtained in common organic solvents. It is desirable to easily prepare flexible and rigid films from solution casting of the material [34, 35]. As shown in Table 1, SPI1 and SPI2 were dissolved in common organic solvents such as *m*-Cresol, DMF, DMSO, NMP, DMac, $CHCl_3$, CH_2Cl_2, acetone, toluene and THF at room temperature. Solubility was determined by taking the ratio of solvent/solute (2% by weight). Resolution and photographs of SPI1 and SPI2 are summarized in Table 1. Both small amounts of SPI1 and SPI2 were insoluble in acetone, toluene and THF. It was observed that SPI1 was slightly soluble in $CHCl_3$ and CH_2Cl_2, but very easily dissolved in NMP, DMac, DMF and DMSO. SPI2 was only slightly soluble in $CHCl_3$, while in CH_2Cl_2, the molecule remained suspended in the solvent as the particle. It

Table 1 Solubility abstracts of SPI1 and SPI2 in known solvents at room temperature

	m-Cresol	DMF	DMSO	NMP	DMac
SPI1	++	++	++	++	++
Photos of Solutions					
	$CHCl_3$	CH_2Cl_2	Acetone	Toluene	THF
SPI1	+	+	-	-	-
Photos of Solutions				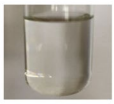	
	DMSO	*m*-Cresol	DMF	DMAc	NMP
SPI2	++	++	++	++	++
Photos of Solutions		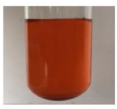			
	$CHCl_3$	CH_2Cl_2	Acetone	Toluene	THF
SPI2	+	+	-	-	-
Photos of Solutions	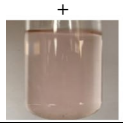	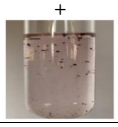			

also dissolved very well in NMP, DMac, DMF and DMSO in SPI2. This means that more CH_3 groups will bring better resolution. Finally, *m*-Cresol solved the SPI1 and SPI2 examples very easily, as it was already used in the synthesis phase.

Solubility parameter and affinity of SPI1 and SPI2

Affinity values have a synergistic effect on increasing the selectivity of polymers [36]. The ion–dipole interactions with polarized oxygen atoms of PIs show an affinity for various chemical species, and this feature can be used in smart sensor design [37]. Solubility parameters of solvents and polymers are needed for the experimental and theoretical calculation of the affinity values of polymers in certain solvents. By calculating the affinity of polymers for solvents, Niknezhad and Jana (2020) stated that miscible solvent pairs with low affinity for one of the polymer components yield core–shell morphology with different polymer interfaces. They also showed that miscible solvent pairs with high affinity for both polymers produced interpenetrating network morphology [38]. In the current studies in the literature, it has been understood that the solubility parameters of the solvents have standard values. However, a separate calculation is required to find the solubility parameter values of unique polymers that are not available in the literature. In this calculation, the molar attraction (F_i) values of each group belonging to the repeating unit of the polymer and its molecular weight and density are used. On the other hand, the densities of polymers that are not available in the literature can be determined by pycnometry. The solubility parameter of the polymer can be calculated by using Eq. 1 based on the studies done.

$$\delta_p = d\Sigma F_i / M_0 \quad (1)$$

Here, δ_p is the solubility parameter of the polymer, d is the density of the polymer, M_0 is the molar mass of the repeating unit, and ΣF_i is the sum of molar attraction [39].

The affinity (ε_p) of a polymer with a particular solvent is calculated using Eq. 2

$$\varepsilon_p = \left(\delta_p - \delta_s\right)^2 \quad (2)$$

Here, ε_p is the affinity value of the polymer, δ_p is the solubility parameter of the polymer, and δ_s is the solubility parameter of the solvent [38].

In this study, it was calculated as d = 1.14 g/cm^3, M_0 = 978 g/mol for SPI1 and d = 1.02 g/cm^3, M_0 = 959 g/mol for SPI2. (Density values were determined by pycnometer method, and acetone was used as liquid.) The Fi values of SPI1 and SPI2 are listed in Table 2. Using these data in Eq. 1, it was calculated as $\delta_p = 22.14$ MPa$^{1/2}$ for SPI1 and $\delta_p = 20.26$ MPa$^{1/2}$ for SPI2. The δ_p values found are close to the δ_p values of polymers known in the literature [38, 40].

The resolution parameter values of the solvents and SPI1 and SPI2, as well as the affinity values of the solvents for SPI1 and SPI2, are listed in Table 3. The ε_p values of SPI1 and SPI2 were calculated using Eq. 2. Here, *m*-Cresol, DMF and DMSO are good solvents for both PI, but the affinity values of SPI1 were lower than those of SPI2. Again, although NMP and DMac are good solvents for the two PIs, the affinity values of SPI1 were even lower than 1. This situation is attributed to the acetamide and pyrrolidone groups. On the other hand, $CHCl_3$, CH_2Cl_2 and acetone

Table 2 Molar attraction values of SPI1 and SPI2 [39, 40]

Group	Fi	Group Number of SPI1	Group Number of SPI2	Total Fi of SPI1 (cal cm^3 mol^{-1})$^{1/2}$	Total Fi of SPI2 (cal cm^3 mol^{-1})$^{1/2}$
C-H	85.99	31	24	2666	2064
-CH = (olefin)	121.53	2	2	243.06	243.06
-CH = (aromatic)	117.12	48	52	5622	6090
-CH = CH-(olefin)	248.0	1	1	248	248
-OH	225.84	2	3	452	678
-N <	62.1	3	3	186.3	186.3
-CHCN	450	9	9	4050	4050
-C-N	360	9	9	3240	3240
-S-	214	3	2	642	428
SO_2	182.83	2	2	366	366
> C = O	262.96	4	4	1052	1052
$-CH_3$	147.3	–	1	–	147.3
5-membered ring	20.99	2	–	42	–
6-membered ring	23.44	8	11	188	258
Total				18,997	19,051

Table 3 Resolution Parameter of Solvents, SPI1 and SPI2 and Corresponding Affinity Values [38, 41, 42]

Solvents and polymers	Solubility parameter ($MPa^{1/2}$)	Affinity of SPI1 (MPa)	Affinity of SPI2 (MPa)
m-Cresol	27.2	25.60	48.16
DMF	24.8	7.07	20.61
DMSO	26.6	19.89	40.19
NMP	22.9	0.57	6.96
DMac	22.7	0.31	5.95
$CHCl_3$	19.0	9.85	1.58
CH_2Cl_2	20.2	3.76	0.03
Acetone	20.3	3.38	0.01
Toluene	18.2	15.52	4.24
THF	19.4	7.50	0.73
SPI1	22.14	–	–
SPI2	20.26	–	–

were not good solvents for either PI and their affinity values were quite low. Again, toluene and THF are not suitable to dissolve the two PIs. But, very interestingly, the values of SPI1 in these two solvents were close to the values in DMSO and DMF. On the contrary, the affinity values of SPI2 are extremely low. In this case, the actual molecular weight (with gel permeation chromatography (GPC)) could not be determined, since the two PIs were insoluble in THF and their affinity values were very low.

UV–Visible spectrums of SPI1 and SPI2

UV–Vis has a significant place in polymer formation and provides clarity in structure lighting [43]. SPI is dissolved in DMF. The optical properties of SPI are examined by measuring with UV–Vis. In the UV–Vis absorption of SPIs, there is strong absorption in DMF solutions, which can be assigned to a p—p* transition [44]. UV–Vis absorption spectrum analysis was performed with five different concentrations of SPI1 and SPI2 in DMF separately. The spectras were showed in Figs. 8 and 9. Herein, 1 ml of solution: (i) 0.02 ml SPI + 0.98 ml DMF, (ii) 0.04 ml SPI + 0.96 ml DMF, (iii) 0.06 ml SPI + 0.94 ml DMF, (iv) 0.08 ml SPI + 0.92 ml DMF and (v) 0.10 ml SPI + 0.90 ml DMF were prepared by applying five versions as. Figure 8 demonstrates the UV–Vis absorption of divergent concentrations of SPI1 in DMF. It presented quintuple absorbance at 290–390 nm in solution of SPI1. Figure 9 demonstrates the UV–Vis absorption of divergent concentrations of SPI2 in DMF. It demonstrated quintuple absorbance at 300–550 nm in solution of SPI2.

TGA/DTA of SPI1 and SPI2

Generally, the results obtained in thermal analyses for SPIs support each other. The temperature values and decay stages represent the SPIs exactly. In studies showing

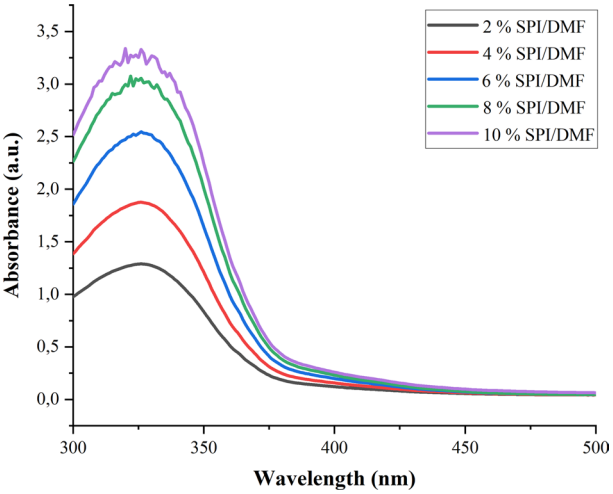

Fig. 8 UV–Vis spectra of SPI1

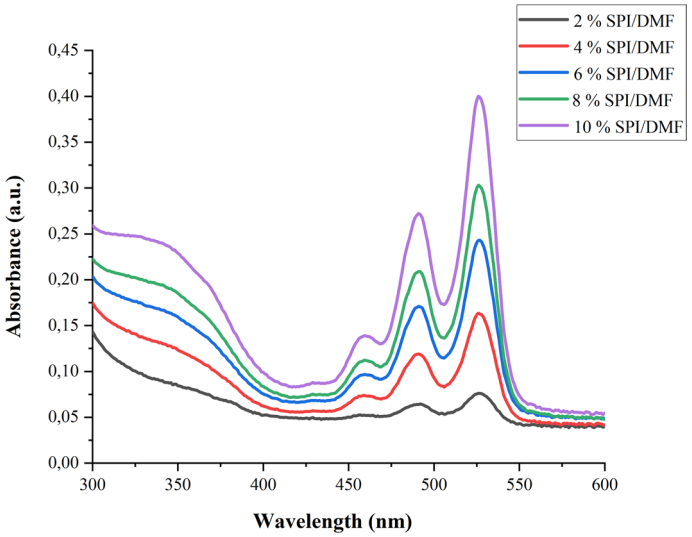

Fig. 9 UV–Vis spectra of SPI2

several different degradation stages according to TGA thermograms of sulfonated polymers, Abu-Orabi et al. noted that the initial weight loss at about 100 °C was due to the evaporation of water molecules absorbed by the highly hygroscopic sulfonic acid groups within the copolymers. They stated that the first degradation step observed around 300 °C corresponds to the degradation of aromatic sulfonyl groups. They concluded that the second weight loss step was observed at a temperature higher than 450 °C and was associated with the degradation of the copolymer

backbone [45]. In studies where three different weight losses were observed according to TGA thermograms of sulfonated polymers, Lee et al. noted that the weight loss around 100 °C was due to loss of residual moisture loss in the polyimide films due to the highly hygroscopic sulfonyl groups. The second step of degradation around 300 °C corresponded to the degradation of aromatic sulfonyl groups. The third step shows the decomposition of the polyimide backbone. In general, all polyimides showed excellent thermal stability (about 500 °C) characteristic of polyimides [46]. According to Yin et al., most of the SPI membranes in their study showed similar thermal stability up to 240–250 °C, resulting from the decomposition of the aliphatic side chain and the sulfonic acid group. Decomposition of the polymer backbone occurred at around 510–530 °C [47].

PTCDA is a very stable compound, and aromatic PIs are special compounds due to their high thermal stability. SPIs are less thermally stable as they exhibit several different degradation steps. Regarding polymer stability, TGA is often used to qualify the temperature of the initial mass loss, which can be seen as the onset of degradation. DTA is performed to show the degradation step exactly. When the DTA curve is entered, the maximum decomposition rate and the corresponding weight loss are seen. It has been observed that the N_2 flow rate in the literature is different in many TGAs. According to Rikukawa et al. in their study, SPIs were investigated by TGA at a heating rate of 10 °C min^{-1} under nitrogen flow [48]. In yet another study, Genies et al. obtained thermogravimetric data both on a TG209 NETZSCH under nitrogen at a heating rate of 5 °C min^{-1} and on a Setaram TGA92 in flowing nitrogen at a heating rate of 1 °C min^{-1} [49]. Therefore, the TGA-DTA curve was evaluated in this study. Thermogravimetric data were taken at a heating rate of 10 °C min^{-1} under nitrogen. TGA-DTA thermograms of SPI1 and SPI2 showed several different decay stages. Figure 10 of SPI1 was presented with detailed data provided by TGA and DTA analyzers. In the curve, the initial weight loss in the

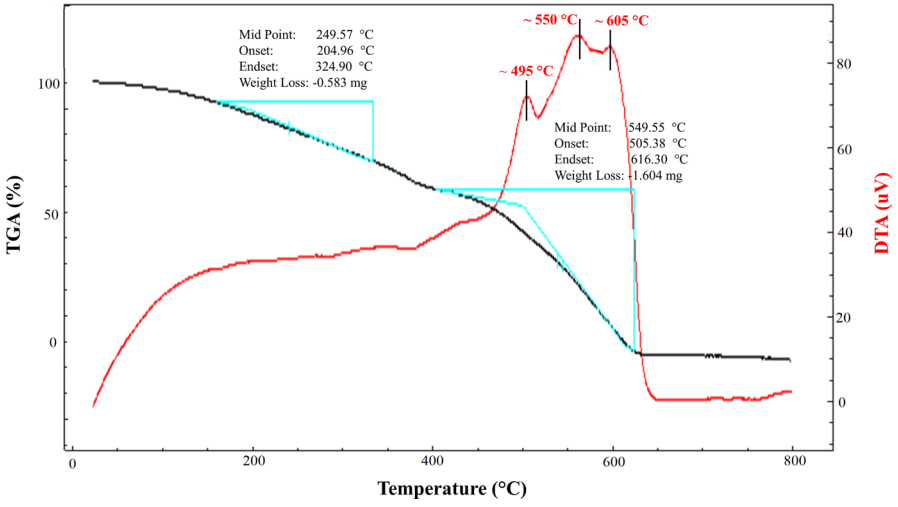

Fig. 10 TGA/DTA curves of SPI1

150–204 °C range corresponds to the elimination of water absorbed by the highly hygroscopic SO3H groups. An important step in the onset of decomposition is the decomposition of sulfonic groups, which leads to the removal of sulfur monoxide and sulfur dioxide gases up to 505 °C. The final stage of degradation corresponds to the polymer backbone above 600 °C. In Fig. 11 with the curve for SPI2, the initial weight loss in the range of 150 °C to 224 °C corresponds to the elimination of water absorbed by the highly hygroscopic SO3H groups. Further weight loss means the removal of the residual m-Cresol solvent in the 428 °C to 497 °C range. An important step at the beginning of decomposition is the decomposition of sulfonic groups, which leads to the removal of sulfur monoxide and sulfur dioxide gases up to 575 °C. The final stage of degradation corresponds to the polymer backbone above 700 °C. Both exothermic and endothermic effects were recorded in the DTA curve of SPI1 and SPI2. The first decomposition observed at about ~ 250 °C may have been caused by the solvent traces. DTA curve has three different peaks of SPI1 in the gas environment. SPI1 has the individual decomposition temperatures as shown in Fig. 10 (roundabout ~ 495 °C, ~ 550 °C and ~ 605 °C, respectively). DTA curve has two broad different peaks of SPI2 in the gas environment (roundabout ~ 395 °C and ~ 550 °C, respectively) as shown in Fig. 11. These results will meet the need for polymer electrolyte membranes that exhibit fast proton transfer at high temperatures, as the synthesized SPIs have higher thermal stability than the intended operating temperature.

Studies of DFT

All DFT studies, including calculating HOMO–LUMO energy levels, have also been calculated and published for SPIs and PIs. For example, Cai et al., (2013) reported that in PIs, Pa showed the highest HOMO and Pc showed the lowest HOMO. They noted

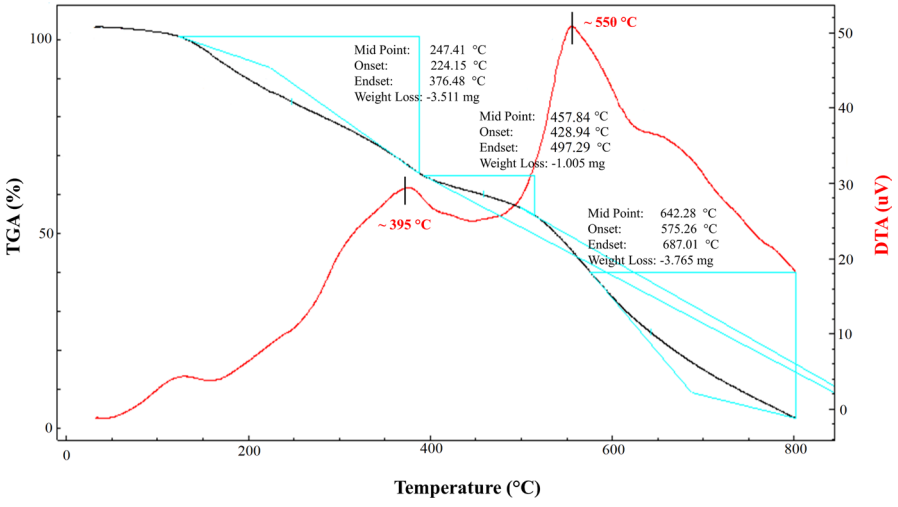

Fig. 11 TGA/DTA curves of SPI2

that the different dianhydride structure plays a key role in the electron structure and regulates the vacancies of PIs [50]. López-Chávez et al., (2014) conducted the study titled "Role of sulfonation in the stability, reactivity and selectivity of poly(ether imide) used to develop ion exchange membranes: DFT study with application to fuel cells." In this study, the chemical structure in the minimum energy state for each simulated SPEI is shown, along with the HOMO and LUMO boundary orbitals. These structures have both polyimide and polyether units in the backbone. SPEIs were obtained by sulfonating PEIs on electron-rich benzene rings [51]. Therefore, molecular dynamics simulation studies were found suitable for SPI. Molecular dynamic simulation studies have been applied to this polymer only at the monomer and oligomer levels.

HOMO and LUMO analysis

HOMO and LUMO energy differences are calculated for each molecule to examine the interaction between SPI and ionic species, and to determine the stability and reactivity degree for each group (between each ionic species and each SPI). The lowest unoccupied molecular orbital creates antibonding for all SPIs [33, 52]. In the figures, the positive phase is shown in blue, while the yellow color represents the negative phase. It shows the values of E_{HOMO} (highest occupied molecular orbital) and E_{LUMO} (lowest unoccupied molecular orbital) [53, 54]. Table 4 and Table S1 give the HOMO and LUMO values. In this study, the volume trajectory of HOMO, LUMO, HOMO-1 and LUMO + 1 for molecules is shown in Figs. 12 and 13. Energy gap (Δ) $|E_{\mathrm{HOMO}} - E_{\mathrm{LUMO}}|$ of SPI1 between one structural unit $|E_{\mathrm{HOMO}} - E_{\mathrm{LUMO}}|$ value is 1.9399 eV, and two structural units' $|E_{\mathrm{HOMO}} - E_{\mathrm{LUMO}}|$ value is 1.998 eV (B3LYP). For SPI2 one structural unit $|E_{\mathrm{HOMO}} - E_{\mathrm{LUMO}}|$ value is 1.568 eV, and two structural units' $|E_{\mathrm{HOMO}} - E_{\mathrm{LUMO}}|$ value is 1.3715 eV (B3LYP). This indicates that both molecules exist stably. Because of their molecular orbitals with similar atomic orbital composition, one- and two-unit oligomers have nearly identical energy levels. As the molecule grew, the HOMO level decreased slightly and the LUMO level increased, which was very small. In this case, the increase in the LUMO level supports proton transfer.

Dipole moment calculations

Molecules showing asymmetric polarization induced by electron donor and acceptor groups in pi-electron conjugated molecules are good candidates for nonlinear optics (NLO) applications in optical signal processing and optical computing. The criteria for a molecule to behave as a good NLO must have a large value of first hyperpolarizability (β) [55]. In this study, the NLO behavior of one and two structural units of SPI1 was determined by determining β, electric dipole moment (μ) and polarizability ($\Delta\alpha$) using B3LYP/6-311G and B3PW91/6-311G(d, p) basis sets examined. The calculated values are listed in Table 5. The magnitude of the total first static β, static dipole moment (μ) and average polarizability ($\Delta\alpha$) in terms of x, y and z components are given in Eqs. 3, 4 and 5 [56].

Table 4 Comparison of the HOMO, LUMO and energy gap properties of one and two structural units of SPI1 and SPI2

Code	Molecules Energy	One structural unit/ B3LYP	Two structural units/ B3LYP
SPI1	E_{LUMO}	− 3.4504	− 3.4278
	E_{HOMO}	− 5.3904	− 5.4258
	E_{LUMO+1}	− 3.0961	− 3.3813
	E_{HOMO-1}	− 6.2277	− 5.5640
	Energy gap (Δ) $\lvert E_{HOMO} - E_{LUMO}\rvert$	1.9399	1.998
	Ionization potential (I = − E_{HOMO})	5.3904	5.4258
	Electron Affinity ($A = -E_{LUMO}$)	3.4504	3.4278
	Chemical hardness ($\eta = (I-A)/2$)	0.9699	0.999
	Chemical softness ($s = 1/2\ \eta$)	0.4849	0.4995
	Chemical Potential ($\mu = -(I+A)/2$)	− 4.4204	− 4.4268
	Electronegativity ($\chi = (1+A)/2$)	2.2252	2.2139
	Electrophilicity index ($\omega = \mu^2/2\ \eta$)	10.0726	9.8080
SPI2	E_{LUMO}	− 3.9269	− 4.1144
	E_{HOMO}	− 5.4949	− 5.4859
	E_{LUMO+1}	− 3.0267	− 3.8820
	E_{HOMO-1}	− 6.4138	− 5.6040
	Energy gap (Δ) $\lvert E_{HOMO} - E_{LUMO}\rvert$	1.568	1.3715
	Ionization potential ($I = -E_{HOMO}$)	5.4949	5.4859
	Electron affinity ($A = -E_{LUMO}$)	3.9269	4.1144
	Chemical hardness ($\eta = (I-A)/2$)	0.784	0.6857
	Chemical softness ($s = 1/2\ \eta$)	0.392	0.3428
	Chemical Potential ($\mu = -(I+A)/2$)	− 4.7109	− 4.8001
	Electronegativity ($\chi = (1+A)/2$)	2.4634	2.5572
	Electrophilicity index ($\omega = \mu^2/2\ \eta$)	14.1533	16.7997

$$\beta top = \left[(\beta xxx + \beta xyy + \beta xzz)^2 + (\beta yyy + \beta yzz + \beta yxx)^2 + (\beta zzz + \beta zxx + \beta zyy)^2 \right]^{1/2} \tag{3}$$

$$\mu = (\mu 2x + \mu 2y + \mu 2z)^{1/2} \tag{4}$$

$$\Delta\alpha = 2^{-1/2} \left[(\alpha xx - \alpha yy)^2 + (\alpha yy - \alpha zz)^2 + (\alpha zz - \alpha xx)^2 + 6\alpha^2 xx \right]^{1/2} \tag{5}$$

One and two structural unit parameters for gas phase compound It was calculated as respectively: μ (D) = 1.1399, 4.5424, 6.5019 and 6.0111, α (au) = 784.78, 690.30, 1703.6 and 1200.5, β (esu) $= 9.4 \times 10^{-35}$, 1.5×10^{-34}, 1.6×10^{-35} and 2.4×10^{-35}. The NLO behavior of one and two structural units of SPI2 was investigated by determining β, μ and $\Delta\alpha$ using the B3LYP/6-311G and

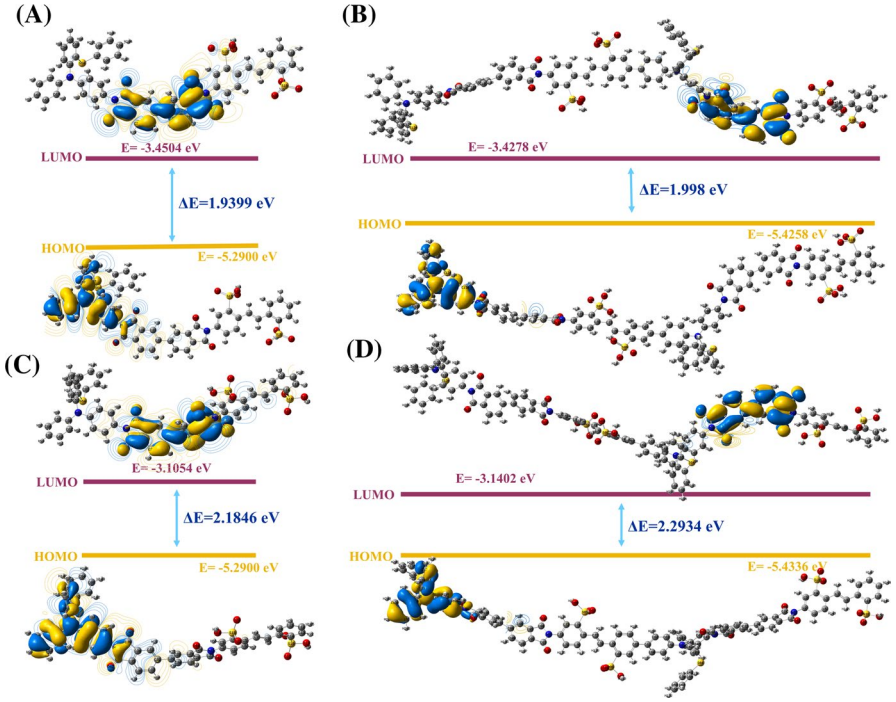

Fig. 12 **A**, **B**, B3LYP and **C**, **D** B3PW91 one structural unit of SPI1 and its two structural units HOMO and LUMO

B3PW91/6-311G(d, p) basis sets. The calculated values are listed in Table 5 and Table S2. High polarity values calculated theoretically from the obtained data were predicted to be good candidates for nonlinear optical materials.

Molecular electrostatic potential (MEP) analysis

Molecular electrostatic potential (MEP) analysis provides valuable evidence about the reactive regions of molecules. MEP can show positive areas associated with nucleophilic attacks (marked in blue) and negative areas associated with electrophilic reactivity (marked in red) [57]. Here, MEP was measured in optimized geometry in B3LYP/6-311G and B3PW91/6-311G (d,p) to find sensitive reactive sites on one and two structural units of SPI1 for electrophilic and nucleophilic attacks. In the MEP map (Fig. 14), the hydrogen atom of SPI1 carries the highest strength of the positive charge in dark blue [58] (6.587 e^{-2}, 6.602 e^{-2}) Maximum carbon and hydrogen atoms were found in the positive region. This indicates that it is a suitable area for nucleophilic attack. Negative (red) regions represent electrophilic reactivity [58] (−6.587 e^{-2}, −6.602 e^{-2}). The majority of the aromatic ring region refers to the green color and is almost neutral.

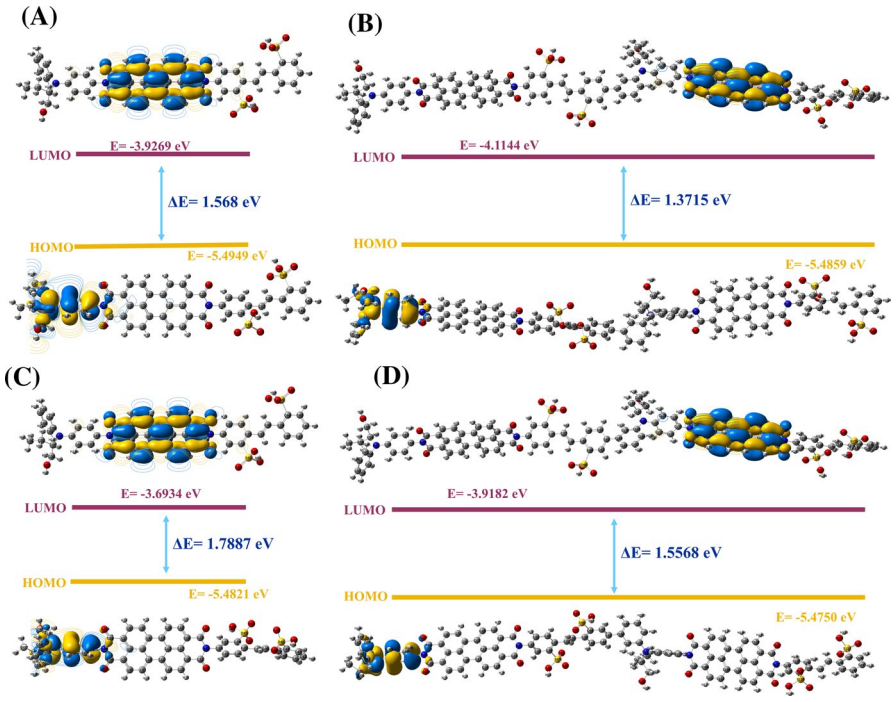

Fig. 13 **A**, **B** B3LYP and **C**, **D** B3PW91 one structural unit of SPI2 and its two structural units HOMO and LUMO

According to these results, the MEP map shows that there are positive potential regions around hydrogen atoms as negative potential regions are on oxygen atoms.

AIM analysis

In AIM analysis, based upon the geometric and topological parameters, it can be deduced that solely hydrogen bonds exist. According to Yildiko et al. (2021) in their work, the remaining BCPs demonstrated feebleness and admit the electrostatic treatment of intermolecular interactions (H ⋯ H, C ⋯ H and C ⋯ C) in the compound [27]. According to Molavian et al. (2016), the structure of the hydrated membrane was optimized to investigate the proton conductivity of the SPI membrane under low humidity conditions. They reported the zero-point energy (ZPE) and binding energy per water molecule based on the ZPE corrected electronic energy for SPI at different hydration states. Proton transfer for SPI occurred in the presence of three water molecules. They showed different configurations of the

Table 5 Dipole moments (Debye), (au) polarizability, β components and β tot. values in the DFT study of the one and two structural units of SPI1 and SPI2

Code	Parameters	One structural unit/B3LYP	Two structural units/B3LYP	Parameters	One structural unit/B3LYP	Two structural units/B3LYP
SPI1	μ_x	0.7914	6.4989	β_{XXX}	271.74	6723.6
	μ_y	−0.4976	0.1467	β_{XXY}	1001.8	1001.2
	μ_z	0.6522	−0.1348	β_{XYY}	61.775	1115.7
	$\mu_{(D)}$	1.1399	6.5019	β_{YYY}	−16.514	385.93
	α_{xx}	−452.28	−730.16	B_{XXZ}	−248.48	1144.6
	α_{yy}	−398.01	−819.28	β_{XYZ}	12.342	354.39
	α_{zz}	−428.69	−880.45	β_{YYZ}	82.897	−38.882
	α_{xy}	−28.698	−23.278	β_{XZZ}	−51.555	−355.96
	α_{xz}	−10.534	64.862	β_{YZZ}	18.551	2.9914
	α_{yz}	−2.7762	−23.511	β_{ZZZ}	17.868	−8.4399
	α(au)	784.78	1703.6	β(esu)	9.4×10^{-35}	1.6×10^{-35}
SPI2	μ_x	−5.0256	2.2552	β_{XXX}	−65.434	7161.0
	μ_y	−0.1100	0.5181	β_{XXY}	−483.07	−1117.6
	μ_z	−0.6405	−0.3140	β_{XYY}	−471.44	466.66
	$\mu_{(D)}$	5.0675	2.3351	β_{YYY}	−1.3914	1.4656
	α_{xx}	−374.54	−660.60	B_{XXZ}	−269.53	−1175.6
	α_{yy}	−438.04	−838.75	β_{XYZ}	23.647	−102.54
	α_{zz}	−422.41	−874.78	β_{YYZ}	63.816	−49.739
	α_{xy}	−25.206	37.095	β_{XZZ}	−25.655	−4.2446
	α_{xz}	39.634	−45.951	β_{YZZ}	−8.5329	66.614
	α_{yz}	5.9624	16.334	β_{ZZZ}	24.252	69.444
	α(au)	651.24	1582.5	β(esu)	1.3×10^{-34}	1.2×10^{-35}

three water molecules around the sulfonate group [59]. In this study, both hydration and proton transfer topology were examined theoretically.

AIM analysis results of hydration status of SPI1 and a structural unit of SPI2

Atoms in molecules (AIM) characterize chemical bonds. In this theory, the critical point (CP) and the bond path (BP) between atoms attached to chemical bonds are always accompanied. Each bond path critical point (BCP) contains well-done chemical information that fully describes the form of the chemical bond. The electron density (ρ_{BCP}), Laplacian of electron density ($\nabla^2 \rho_{BCP}$), potential energy density (V_{BCP}), kinetic energy density (G_{BCP}), electronic energy density (H_{BCP}) and ellipticity (δ) are parameters [57, 60, 61]. Molecular graphs of functionalized SPI1 and a structural unit of SPI2 with hydrates are shown in Fig. 15. A structural unit of SPI1 and SPI2 at various hydration states of the acidic proton of the OH group was analyzed in the program and reported in Tables S3 and S4. When

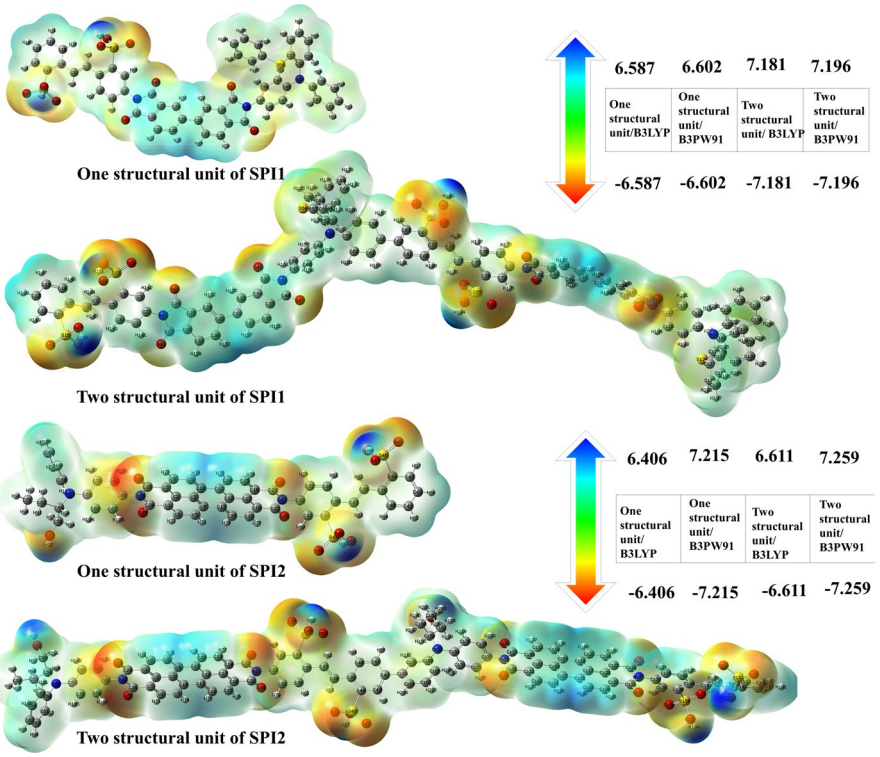

Fig. 14 MEP analysis maps of the one and two structural units of SPI1 and SPI2

the water molecule was added, it retained the covalent character of the acidic O–H, retaining the hydrogen atom and not being separated by the oxygen of the sulfonate group. However, when 1, 2 and 3 H_2O molecules were added, separation of acidic H^+ occurred in all three cases. However, as much as the strong H bond between the oxygen of the sulfonate group and the H_3O^+ produced, proton transfer was done. The V_{BCP}, H_{BCP} and $\nabla^2 \rho_{BCP}$ values showed that the HB energy and covalent character of O–H decreased with the increase in the number of water molecules. With the increase of water molecules, the H_{BCP} value of one structural unit of SPI1 was reduced from + 0.496051 to − 0.002746 a.u. and the $\nabla^2 \rho_{BCP}$ value was also reduced from + 0.061530 to − 1.903610 a.u. On the other hand, the H_{BCP} value of one structural unit of SPI2 was reduced from + 0.496074 to − 0.002500 a.u. and the $\nabla^2 \rho_{BCP}$ value was reduced from + 0.061394 to − 1.849548 a.u. As a result, proton transfer was easier in states of superior hydration.

In addition, the water molecules were able to properly stabilize the hydrogen bond (HB) formation (in the presence of nitrogen atoms) by the hydronium ion, thus

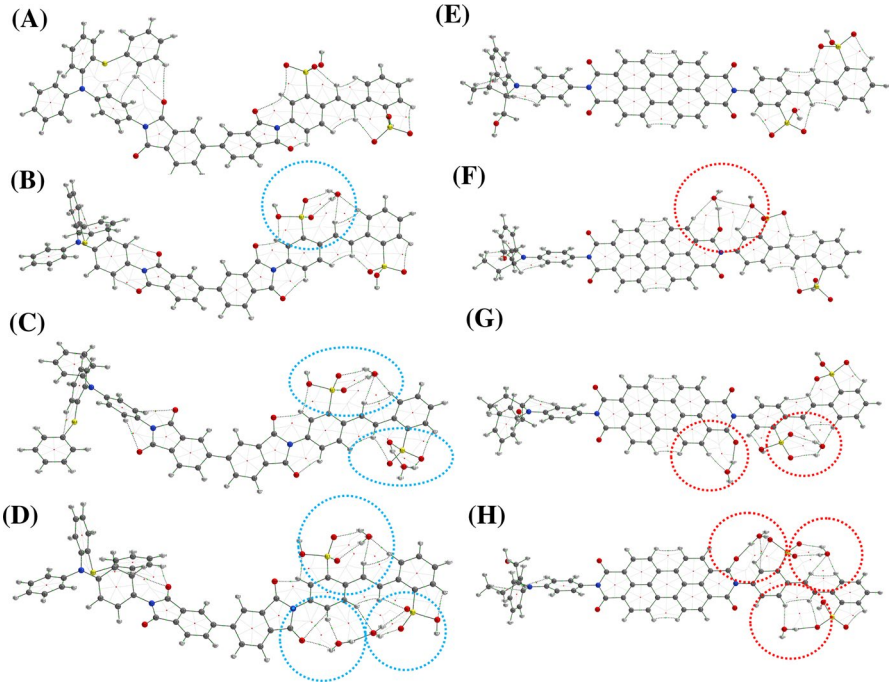

Fig. 15 Dry one structural unit of SPI1 (**A**) and SPI2 (**E**), hydrated one structural unit of SPI1 (**B**) and SPI2 (**F**) at the level of one water molecule, hydrated one structural unit of SPI1 (**C**) and SPI2 (**G**) at the level of two water molecules, hydrated one structural unit of SPI1 (**D**) and SPI2 (**H**) at the level of three water molecules

facilitating proton transfer. In addition, hydrogen bonds between the oxygen atom of the sulfonate group and water molecules with hydrogen atoms were investigated.

Conclusions

Diamine 1 and diamine 2 were synthesized in the presence of CsF and DMSO with 67% and 66% yields in the presence of Pd/C (10%) and EtOH. Then, SPI1 and SPI2 with two different high-performance properties were synthesized by the thermal solution imidization method of polyamic acid. Solubility tests were performed on synthesized SPI1 and SPI2 with various spectroscopic analyses and in various solvents. The solubility parameter values of the solvents and SPI1 and SPI2, as well as the affinity values of the solvents for SPI1 and SPI2, were calculated. The quantum chemistry calculations were performed in DFT studies (calculations of HOMO–LUMO energies, dipole moment calculations, MEP analysis) on the B3LYP/6-311G and B3PW91/6-311G (d,p) basis sets separately for different unit oligomers of SPI1 and SPI2. When the computational chemistry values of the different oligomers of both polymers are compared, it can be interpreted

that there is not much difference. AIM analysis, which is another theoretical modeling, was evaluated by applying it to a different number of units of SPI1 and SPI2 in the same way. The hydrated molecular of a structural unit of SPI1 and SPI2 was analyzed at various hydration states in the BCP of the acidic proton of the OH group. As a result, proton transfer was easier in states of hydration. In line with these evaluations, it was concluded that the proton transfer and water retention potentials of the synthesized SPIs were high.

Supplementary Information The online version contains supplementary material available at https://doi.org/10.1007/s00289-022-04536-0.

Declarations

Conflict of interest The authors declare that there is no conflict of interest in the work reported in this article.

References

1. McKeen L (2012) 6 - Polyimides. In: McKeen L (ed) The effect of sterilization on plastics and elastomers, 3rd edn. William Andrew Publishing, Boston
2. Massey LK (2003) Chapter 33 - polyimide. In: Massey LK (ed) Permeability properties of plastics and elastomers, 2nd edn. William Andrew Publishing, Norwich, NY
3. Kayvani Fard A, McKay G, Buekenhoudt A, Al Sulaiti H, Motmans F, Khraisheh M, Atieh M (2018) Inorganic membranes: preparation and application for water treatment and desalination. Materials (Basel) 11:74. https://doi.org/10.3390/ma11010074
4. Lee T, Park SS, Jung Y, Han S, Han D, Kim I, Ha C-S (2009) Preparation and characterization of polyimide/mesoporous silica hybrid nanocomposites based on water-soluble poly(amic acid) ammonium salt. Eur Polym J 45:19–29. https://doi.org/10.1016/j.eurpolymj.2008.09.022
5. Volksen W (1994) Condensation polyimides: synthesis, solution behavior, and imidization characteristics. In: Hergenrother PM (ed) High performance polymers. Springer, Berlin Heidelberg, Berlin, Heidelberg
6. Lee J, Baek S, Kim J, Lee S, Kim J, Han H (2021) Highly soluble fluorinated polyimides synthesized with hydrothermal process towards sustainable green technology. Polymers 13:3824. https://doi.org/10.3390/polym13213824
7. Feng X, Liu J (2018). Thermoplastic Polyimide (TPI). In: High Performance Polymers and Their Nanocomposites Hobon, NJ USA, John Wiley PP. 149-219
8. Deng B, Zhang S, Liu C, Li W, Zhang X, Wei H, Gong C (2018) Synthesis and properties of soluble aromatic polyimides from novel 4,5-diazafluorene-containing dianhydride. RSC Adv 8:194–205. https://doi.org/10.1039/C7RA12101F
9. Nunes SP (2008) Organic-inorganic membranes. In: membrane science and technology, vol 13. Elsevier, pp 121–134. https://doi.org/10.1016/S0927-5193(07)13004-7
10. Weber AZ, Newman Jo (2007) Macroscopic modeling of polymer-electrolyte membranes. Advances in fuel cell. Elsevier. https://doi.org/10.1016/S1752-301X(07)80007-X
11. Li X (2007) Chapter One - Thermodynamic Performance of Fuel Cells and Comparison with Heat Engines. In: Zhao TS, Kreuer KD, Van Nguyen T (eds) Advances in fuel cells, vol 1. Elsevier Science, https://doi.org/10.1016/S1752-301X(07)80006-8
12. Mahdavi H, Ahmadian-Alam L (2015) 32.Sulfonic acid functionalization of 2-aminoterephthalate metal−organic framework and silica nanoparticles by surface initiated radical polymerization: as proton-conducting solid electrolytes. J Polym Res. https://doi.org/10.1007/s10965-015-0708-4
13. Hooshyari K, Rezania H, Vatanpour V, Salarizadeh P, Askari MB, Beydaghi H, Enhessari M (2020) High temperature membranes based on PBI/sulfonated polyimide and doped-perovskite nanoparticles for PEM fuel cells. J Membr Sci 612:118436. https://doi.org/10.1016/j.memsci.2020.118436

14. Akbarian-Feizi L, Mehdipour-Ataei S, Yeganeh H (2010) Survey of sulfonated polyimide membrane as a good candidate for nafion substitution in fuel cell. Int J Hydrog Energy 35:9385–9397. https://doi.org/10.1016/j.ijhydene.2010.03.072
15. Lee CH, Park CH, Lee YM (2008) Sulfonated polyimide membranes grafted with sulfoalkylated side chains for proton exchange membrane fuel cell (PEMFC) applications. J Membr Sci 313:199–206. https://doi.org/10.1016/j.memsci.2008.01.004
16. Ryu T, Sutradhar SC, Ahmed F, Choi K, Yang H, Yoon S, Lee S, Kim W (2017) Synthesis and characterization of sulfonated mutiphenyl conjugated polyimide for PEMFC. J Ind Eng Chem 49:99–104. https://doi.org/10.1016/j.jiec.2017.01.013
17. Wang L, Yi BL, Zhang HM, Liu YH, Xing DM, Shao ZG, Cai YH (2007) Sulfonated polyimide/PTFE reinforced membrane for PEMFCs. J Power Sour 167:47–52. https://doi.org/10.1016/j.jpowsour.2006.12.111
18. Nguyen TH, Wang C, Wang X (2009) Pore-filling membrane for direct methanol fuel cells based on sulfonated poly(styrene-ran-ethylene) and porous polyimide matrix. J Membr Sci 342:208–214. https://doi.org/10.1016/J.MEMSCI.2009.06.042
19. Dudowicz J, Freed KF, Douglas JF (2015) Theory of competitive solvation of polymers by two solvents and entropy-enthalpy compensation in the solvation free energy upon dilution with the second solvent. J Chem Phys 142:214906. https://doi.org/10.1063/1.4921373
20. Shireen Z, Babu SB (2018) Cage dynamics leads to double relaxation of the intermediate scattering function in a binary colloidal system. Soft Matter 14:9271–9281. https://doi.org/10.1039/C8SM01474D
21. Hansen CM (2004) 50 Years with solubility parameters—past and future. Prog Org Coat 51:77–84. https://doi.org/10.1016/j.porgcoat.2004.05.004
22. Hildebrand JH, Scott RL (1964) The solubility of nonelectrolytes. Dover Publications
23. Cousins KR (2005) ChemDraw Ultra 9.0. cambridgesoft, 100 cambridgepark Drive, Cambridge, MA 02140. www. cambridgesoft.com. see web site for pricing options. J Am Chem Soc 127:4115–4116. https://doi.org/10.1021/ja0410237
24. Frisch M, Trucks G, Schlegel H, Scuseria G, Robb M, Cheeseman J, Scalmani G, Barone V, Petersson G, Nakatsuji H (2016) Gaussian 16. Gaussian, Inc. Wallingford, CT, E.U.A.
25. Keith T (2011) AIMAll (standard mode). Version 11(02):27
26. Khalid N, Bibi A, Akhtar K, Mustafa K, Khan M, Saeed N (2019) New Blue Light Emissive polyazomethine(S) containing Bromo-triphenyl units: synthesis and photophysics. Polym-Plast Tech Mat 58:419–426. https://doi.org/10.1080/03602559.2018.1471719
27. Yildiko Ü, Türkan F, Tanriverdi AA, Ata AC, Atalar MN, Cakmak İ (2021) Synthesis, enzymes inhibitory properties and characterization of 2- (bis (4-aminophenyl) methyl) butan-1-ol compound: quantum simulations, and in-silico molecular docking studies. J Indian Chem Soc 98:100206. https://doi.org/10.1016/j.jics.2021.100206
28. Utracki LA (2014) 2_Characterization methods for high temperature polymer blends. high temperature polymer blends. Elsevier, pp 14–69. https://doi.org/10.1533/9780857099013.14
29. CagriAta A, Yildiko Ü, Cakmak İ, Tanriverdi AA (2021) Synthesis and characterization of polyvinyl alcohol-g-polystyrene copolymers via MADIX polymerization technique. Iran Polym J 30:885–895. https://doi.org/10.1007/s13726-021-00940-x
30. Yildiko U, Ata AC, Cakmak İ, Tanriverdi AA (2021) The polyethylene glycol xanthate-mediated synthesis of block copolymers via novel MADIX agents containing azo initiator: effect of PEG chain length on molecular properties. Polym Bull. https://doi.org/10.1007/s00289-021-03813-8
31. Utracki LA (2014) Characterization of high temperature polymer blends for specific applications: fuel cells and aerospace applications. high temperature polymer blends. Elsevier, pp 70–129. https://doi.org/10.1533/9780857099013.70
32. Sahoo S, Chakraborti C, Behera P, Mishra S (2012) FTIR and raman spectroscopic investigations of a Norfloxacin/Carbopol934 polymeric suspension. J Young Pharm 4:138–145. https://doi.org/10.4103/0975-1483.100017
33. Yİldİko Ü, Ata AÇ, Tanriverdİ AA, Çakmak İ, (2021) Investigation of novel diethanolamine dithiocarbamate agent for RAFT polymerization: DFT computational study of the oligomer molecules. Bull Mater Sci 44:186. https://doi.org/10.1007/s12034-021-02450-1
34. Zhang D, Seong JG, Lee WH, Ando S, Wan Y, Lee YM, Zhuang Y (2020) Effects of sulfonate incorporation and structural isomerism on physical and gas transport properties of soluble sulfonated polyimides. Polymer 191:122263. https://doi.org/10.1016/j.polymer.2020.122263

35. Yildiko U, Tanriverdi AA (2021) Synthesis and characterization of pyromellitic dianhydride based sulfonated polyimide: survey of structure properties with DFT and QTAIM. J Polym Res 29:19. https://doi.org/10.1007/s10965-021-02872-9
36. Xu X, Wang J, Dong J, Li H-B, Zhang Q, Zhao X (2020) Ionic polyimide membranes containing Tröger's base: synthesis, microstructure and potential application in CO2 separation. J Membr Sci 602:117967. https://doi.org/10.1016/j.memsci.2020.117967
37. Chiriac A-P, Damaceanu M-D (2021) A novel approach towards crown-ether modified polyimides with affinity for alkali metal ions recognition. J Mol Liq 322:114929. https://doi.org/10.1016/j.molliq.2020.114929
38. Niknezhad S, Jana SC (2020) Bicomponent nanofibers from core–shell nozzle in gas jet spinning process. J Appl Polym Sci 137:48901. https://doi.org/10.1002/app.48901
39. Van Krevelen DW, Te Nijenhuis K (2009) Cohesive properties and solubility. Properties of polymers. Elsevier. https://doi.org/10.1016/B978-0-08-054819-7.00007-8
40. Stefanis E, Panayiotou CJIjop, (2012) A new expanded solubility parameter approach. Int J Pharm 426(1–2):29–43. https://doi.org/10.1016/j.ijpharm.2012.01.001
41. Hansen CM (2007) Hansen solubility parameters: a user's handbook. CRC Press
42. Mark JE (2009) Polymer data handbook. Oxford University Press
43. Antosiewicz JM, Shugar D (2016) UV-Vis spectroscopy of tyrosine side-groups in studies of protein structure. Part 2: selected applications. Biophys Rev 8:163–177. https://doi.org/10.1007/s12551-016-0197-7
44. Dokládalová L, Bureš F, Kuznik W, Kityk IV, Wojciechowski A, Mikysek T, Almonasy N, Ramaiyan M, Padělková Z, Kulhánek J, Ludwig M (2014) Dicyanobenzene and dicyanopyrazine derived X-shaped charge-transfer chromophores: comparative and structure–property relationship study. Org Biomol Chem 12:5517–5527. https://doi.org/10.1039/C4OB00901K
45. Abu-Orabi FM, Kailani MH, Sweileh BA, Mustafa MY, Al-Hussein MJPB (2017) Sulfonated polyimide copolymers based on 4, 4′-diaminostilbene-2, 2′-disulfonic acid and 3, 5, 3′, 5′-tetramethylbenzidine with enhanced solubility. Polym Bull 74:895–909. https://doi.org/10.1007/s00289-016-1752-x
46. Lee C, Sundar S, Kwon J, Han H (2004) Structure–property correlations of sulfonated polyimides. II. effect of substituent groups on membrane properties. J Polym Sci A Polym Chem 42:3621–3630. https://doi.org/10.1002/pola.20215
47. Yin Y, Du Q, Qin Y, Zhou Y, Okamoto K-i (2011) Sulfonated polyimides with flexible aliphatic side chains for polymer electrolyte fuel cells. J Membr Sci 367:211–219. https://doi.org/10.1016/j.memsci.2010.10.054
48. Rikukawa M, Sanui KJPiPS, (2000) Proton-conducting polymer electrolyte membranes based on hydrocarbon polymers. Prog Polym Sci 25:1463–1502. https://doi.org/10.1016/S0079-6700(00)00032-0
49. Genies C, Mercier R, Sillion B, Cornet N, Gebel G, Pineri M (2001) Soluble sulfonated naphthalenic polyimides as materials for proton exchange membranes. Polymer 42:359–373. https://doi.org/10.1016/S0032-3861(00)00384-0
50. Cai J, Ma L, Niu H, Zhao P, Lian Y, Wang W (2013) Near infrared electrochromic naphthalene-based polyimides containing triarylamine: Synthesis and electrochemical properties. Electrochim Acta 112:59–67. https://doi.org/10.1016/j.electacta.2013.08.160
51. López-Chávez E, Peña-Castañeda YA, de la Portilla-Maldonado LC, Guzmán-Pantoja J, Martínez-Magadán JM, Oviedo-Roa R, de Landa C-A, Cruz-Torres A (2014) Role of sulfonation in the stability, reactivity, and selectivity of poly(ether imide) used to develop ion exchange membranes: DFT study with application to fuel cells. J Mol Model 20:2325. https://doi.org/10.1007/s00894-014-2325-2
52. Yildiko U, Tanriverdi AA (2022) A novel sulfonated aromatic polyimide synthesis and characterization: Energy calculations. BKCS n/a, Wiley Online Library, QTAIM simulation study of the hydrated structure of one unit. https://doi.org/10.1002/bkcs.12521
53. Özdemir N, Eren B, Dinçer M, Bekdemir Y (2010) Experimental and ab initio computational studies on 4-(1H-benzo[d]imidazol-2-yl)-N, N-dimethylaniline. Mol Phys 108:13–24. https://doi.org/10.1080/00268970903476688
54. Buvaneswari M, Santhakumari R, Usha C, Jayasree R, Sagadevan S (2021) Synthesis, growth, structural, spectroscopic, optical, thermal, DFT, HOMO–LUMO, MEP, NBO analysis and thermodynamic properties of vanillin isonicotinic hydrazide single crystal. J Mol Struct 1243:130856. https://doi.org/10.1016/j.molstruc.2021.130856

55. Doneux T, Tielens F, Geerlings P, Buess-Herman C (2006) Experimental and density functional theory study of the vibrational properties of 2-Mercaptobenzimidazole in interaction with Gold. J Phys Chem A 110:11346–11352. https://doi.org/10.1021/jp061582v
56. Włodarska M, Mossety-Leszczak B (2021) DFT studies of selected epoxies with mesogenic Units-impact of molecular structure on electro-optical response. Int J Mol Sci 22:3424. https://doi.org/10.3390/ijms22073424
57. Kargar H, Fallah-Mehrjardi M, Behjatmanesh-Ardakani R, Munawar KS, Ashfaq M, Tahir MN (2022) Diverse coordination of isoniazid hydrazone Schiff base ligand towards iron(III): synthesis, characterization, SC-XRD, HSA, QTAIM, MEP, NCI, NBO and DFT study. J Mol Struct 1250:131691. https://doi.org/10.1016/j.molstruc.2021.131691
58. Raissi H, Khoshbin Z, Mollania F (2014) The analysis of structural and electronic properties for assessment of intramolecular hydrogen bond (IMHB) interaction: a comprehensive study into the effect of substitution on intramolecular hydrogen bond of 4-nitropyridine-3-thiol in ground and electronic excited state. Struct Chem 25:515–538. https://doi.org/10.1007/s11224-013-0314-1
59. Molavian MR, Abdolmaleki A, Eskandari K (2016) Theoretical investigation of proton-transfer in different membranes for PEMFC applications in low humidity conditions. Comput Mater Sci 122:126–138. https://doi.org/10.1016/j.commatsci.2016.05.003
60. Gupta VP (2016) Topological analysis of electron density quantum theory of atoms in molecules. Princ Appl Quantum Chem. https://doi.org/10.1016/B978-0-12-803478-1.00011-X
61. Abdolmaleki A, Eskandari K, Molavian MRJP (2016) Sulfonated or phosphonated membranes? DFT investigation of proton exchange in poly (oxadiazole) membranes. Polymer 87:181–193. https://doi.org/10.1016/j.polymer.2016.02.011